5-1-2023

Improper ferroelectricity in ultrathin hexagonal ferrites films

Xin Li

Yu Yun

X. S. Xu

Applied Physics Letters ARTICLE scitation.org/journal/apl

Improper ferroelectricity in ultrathin hexagonal ferrites films

Cite as: Appl. Phys. Lett. **122**, 182901 (2023); doi: 10.1063/5.0146420
Submitted: 13 February 2023 · Accepted: 19 April 2023 ·
Published Online: 1 May 2023

Xin Li,[1] Yu Yun,[1] and Xiaoshan Xu[1,2,a)]

AFFILIATIONS

[1]Department of Physics and Astronomy, University of Nebraska, Lincoln, Nebraska 68588, USA
[2]Nebraska Center for Materials and Nanoscience, University of Nebraska, Lincoln, Nebraska 68588, USA

[a)]Author to whom correspondence should be addressed: xiaoshan.xu@unl.edu

ABSTRACT

Suppression of ferroelectricity in ultrathin films of improper ferroelectric hexagonal ferrites or manganites has been attributed to the effect of interfacial clamping; however, the quantitative understanding and related phenomenological model are still lacking. In this work, we report on the paraelectric-to-ferroelectric phase transition of epitaxial h-$ScFeO_3$ films with different thicknesses through *in situ* reflection high-energy electron diffraction. Based on the interfacial clamping model and the Landau theory, we show that the thickness-dependence of the ferroelectric Curie temperature can be understood in terms of the characteristic length of an interfacial clamping layer and the bulk Curie temperature. Furthermore, we found that the critical thickness of improper ferroelectricity is proportional to the characteristic length of the interfacial clamping layer. These results reveal the essential role of mechanical clamping from interface on the improper ferroelectricity of hexagonal ferrites or manganites and could serve as the guidance to achieve robust improper ferroelectricity in ultrathin films.

Two-dimensional (2D) ferroelectricity has recently attracted intensive research interest due to mechanisms for stabilizing polar order as well as their potentials to device scalability.[1–3] In principle, epitaxial films of bulk ferroelectrics can also be scaled down to several unit cells. However, for proper ferroelectrics of perovskite structures, such as $BaTiO_3$ (BTO) and $PbTiO_3$ (PTO),[4–8] if the depolarization field is not fully screened, there may exist critical thickness below which ferroelectricity is quenched. This critical-thickness problem can be alleviated in improper ferroelectrics. For example, in improper ferroelectric hexagonal manganites (h-$RMnO_3$, R = Sc, Y, and Ho-Lu) or ferrites (h-$RFeO_3$), ferroelectric order originates from coupling of polarization with non-polar structural distortion. This mechanism enables improper ferroelectricity in the ultrathin limit,[9–11] which is comparable to the thickness of 2D ferroelectrics with only a few atomic layers.[12–15]

On the other hand, recent studies revealed an interfacial clamping layer in hexagonal manganite and ferrite thin films,[10,11] which may significantly affect the ferroelectricity in the ultrathin limit. The transition temperature from a paraelectric phase to a ferroelectric phase was observed to decrease with reducing thickness, and the interfacial clamping effect suppresses polarization within the first 2 unit cells (uc) in an h-$RMnO_3$ film.[10] Despite these observations, how the interfacial layer determines the temperature and thickness dependence of ferroelectricity has not been studied systematically, and the ultrathin films of h-$RFeO_3$ could provide the chance to further clarify the general role of the interfacial clamping layer.

Improper ferroelectric h-$RFeO_3$ is formed by a triangle lattice of FeO_5 bipyramids sandwiched by rare earth layers.[16,17] The triangle lattice of FeO_5 rotates 60° for alternative half unit cell, as shown in Fig. 1(a). The collective tilt of FeO_5 bipyramids corresponds to the K_3 mode distortion. The K_3 mode causes the imbalanced displacements of rare-earth ions along the c axis (Γ_2^- mode), leading to the ferroelectricity in h-$RFeO_3$. The ferroelectricity is called improper since the primary order parameters are (Q, ϕ_Q), in which Q is the magnitude mode and ϕ_Q is the tilt angle of the FeO_5 bipyramids. The induced spontaneous polarization is proportional to $Q^3\cos(3\phi_Q)$ in h-$RFeO_3$.

As shown in Fig. 1(b), below T_c, the energy landscape of ferroelectric h-$RFeO_3$ is Mexican-hat shape with sixfold symmetry based on the Landau theory.[18] For the ground states, the order parameter ϕ_Q can only take discrete values $\frac{n\pi}{3}$, where n is integer. When the temperature increases, the magnitude of Q for the ground states decreases gradually, which also leads to suppression of polarization.[19] Above T_c, the ferroelectric phase transforms to the paraelectric phase ($Q = 0$), as shown in Fig. 1(c) based on the Landau theory. In addition, although the theory predicts no critical thickness in improper ferroelectric hexagonal ferrites and manganites,[9] recent experimental study indicates a

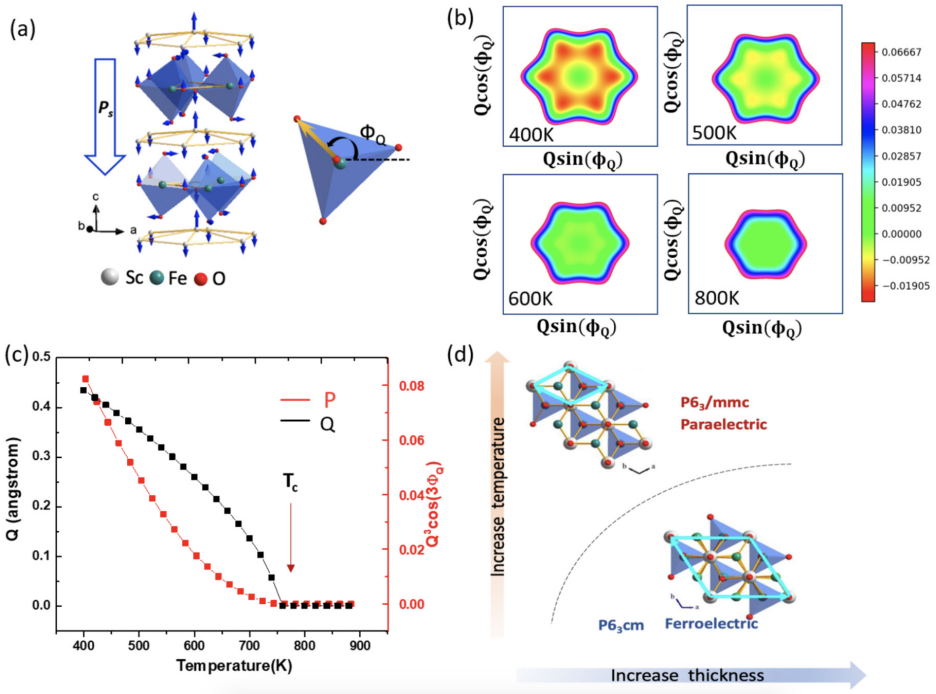

FIG. 1. (a) Atomic structure of h-RFeO$_3$ and the rotation angle of apical oxygen atoms (ϕ_Q). (b) Representative energy landscapes of h-RFeO$_3$ at different temperatures, assuming T_c as 750 K. (c) The temperature dependence of the order parameter Q and the polarization $P = Q^3\cos(3\phi_Q)$ for bulk-state h-RFeO$_3$ based on the Landau theory. (d) Schematic diagrams for the temperature and thickness driven phase transition in h-RFeO$_3$ films and related atomic structures in the a–b plane.

thickness-driven ferroelectric-to-paraelectric transition due to the interfacial clamping of Q to a substrate,[10] as depicted in Fig. 1(d). While the thermally driven transition is intrinsic to the temperature dependence of free energy, the thickness-driven transition is expected to be an extrinsic effect due to the elastic disruption of polar order at the film/substrate interface.

Here, we focus on h-ScFeO$_3$ films, in which the smaller radius of Sc ions leads to larger K_3 distortion with $Q \approx 1$ Å, compared with other hexagonal ferrites such as h-LuFeO$_3$ and h-YbFeO$_3$.[20,21] We show that T_c of the h-ScFeO$_3$ films, inferred from characteristic diffraction streaks of the *in situ* reflection high-energy electron diffraction (RHEED) patterns, decreases when the film thickness reduces. The thickness dependence of T_c and a critical thickness of ferroelectricity (ζ_{FE}) can be well modeled with the Landau theory using the characteristic length of the interfacial clamping layer (ζ_0) and the bulk Curie temperature (T_S) as two key parameters. These results elucidate that, in hexagonal ferrites and manganites, the interfacial-clamping-originated critical thickness is expected to affect scalability in ultrathin films.

To reveal the origin of thickness-dependent scaling of T_c, the epitaxial h-ScFeO$_3$ films with different thicknesses were grown on Al$_2$O$_3$ (0001) and SrTiO$_3$ (111) substrates by pulsed laser deposition (PLD) with a KrF excimer laser (248 nm and 2 Hz repetition rate). For every half unit cell, the h-ScFeO$_3$ films were first grown at 650 °C and then annealed at 850 °C under an oxygen pressure of 10 mTorr to achieve high crystallinity.[21] As shown in Fig. 2(a), in the 2θ scans within the range of 10°–70°, only peaks of h-ScFeO$_3$ films (in addition to substrate peaks) along the [000l] direction can be identified on both Al$_2$O$_3$ (0001) and SrTiO$_3$ (STO) (111) substrates. Moreover, the in-plane epitaxy relationship can be inferred by comparing the RHEED patterns of a film with a substrate in Fig. 2(b). Specifically, the in-plane [100] direction of the h-ScFeO$_3$ film is parallel to [11$\bar{2}$0] of Al$_2$O$_3$ and [$\bar{2}$11] of STO, respectively. The characteristic RHEED pattern for h-ScFeO$_3$ is also consistent with a minimal impurity phase. The thickness-dependent lattice constant c increases with the increase in thickness, as shown in Fig. S1 of the supplementary material, indicating that the h-ScFeO$_3$ film is under in-plane tensile strain on both substrates.

In h-RFeO$_3$, the paraelectric-to-ferroelectric phase transition is accompanied by tripling of the in-plane unit cell for the ferroelectric phase ($P6_3cm$) compared with the paraelectric phase ($P6_3/mmc$), as illustrated in Fig. 1(d). Since the separation of the RHEED streaks is inversely proportional to the in-plane lattice constant,[22] RHEED patterns with the electron beam along the h-ScFeO$_3$ [100] direction provide measurements for the tripled unit cell of the ferroelectric phase with $P6_3cm$ symmetry. Specifically, the RHEED pattern of the paraelectric phase consists of the (0,0) and ($\pm n$,0) diffraction streaks. The tripled in-plane unit cell of the ferroelectric phase leads to the formation of weaker diffraction streaks at the $\pm(3n+1)/3$ and $\pm(3n+2)/3$ positions along the h-ScFeO$_3$ [001] direction,[23] as shown in Fig. 2(b).

Figures 3(a)–3(c) display the RHEED patterns of 2, 5, and 17 unit cell (uc) h-ScFeO$_3$/Al$_2$O$_3$ films, respectively, which were captured at room temperature after growth, below which are the normalized line profiles of the RHEED intensity after integrating along the vertical direction with background subtracted. The *in situ* RHEED images were captured with the decrease in temperature from growth temperature to room temperature. For the 17 uc film, the intensity of the weak streaks gradually increases when the temperature reaches below ~670 K, indicating the temperature-driven paraelectric-to-ferroelectric phase transition. When the thickness is 2 uc, as shown in Fig. 3(a), no weak streaks could be identified down to room temperature. The missing weak streaks in the 2 uc film suggest that the mechanical boundary

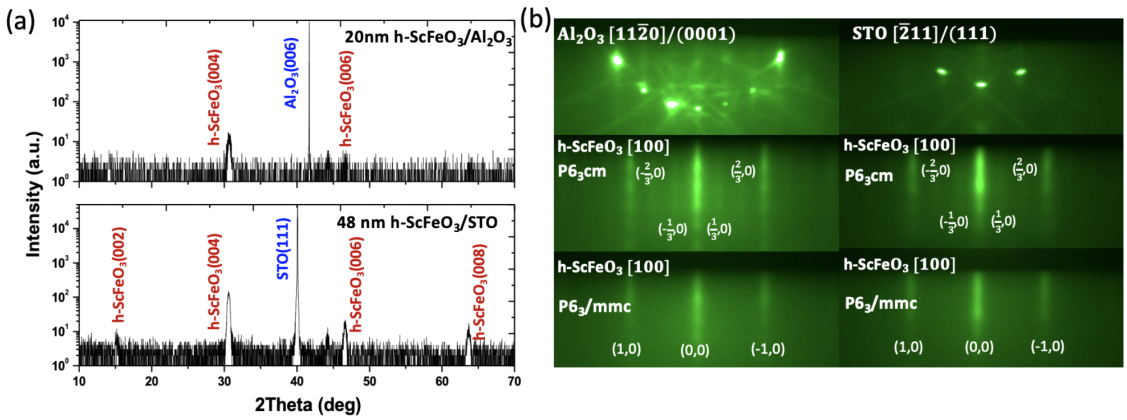

FIG. 2. (a) 2θ scan for 20 nm h-$ScFeO_3/Al_2O_3$ and 48 nm h-$ScFeO_3$/STO films. (b) RHEED patterns of the ferroelectric phase ($P6_3cm$ symmetry) and the paraelectric phase ($P6_3/mmc$ symmetry) and in-plane epitaxy relationships for h-$ScFeO_3/Al_2O_3$ and h-$ScFeO_3$/STO films. The RHEED pattern for Al_2O_3 and STO substrates (top row) were captured at 650 °C before deposition. Middle and bottom rows are the RHEED patterns for h-$ScFeO_3$ captured at room temperature and 650 °C, respectively. The thickness is 17 and 21 uc for h-$ScFeO_3/Al_2O_3$ and h-$ScFeO_3$/STO, respectively.

conditions at the interface or interfacial clamping may modify the energy-minimum state, considering that previously reported epitaxial thin films of hexagonal ferrite or mangnites exhibit the full suppression of K_3 distortion in the interfacial layer.[10,11]

To trace the change of T_c with respective to the film thickness, the *in situ* RHEED images were captured during post-growth cooling; the temperature dependence of the RHEED intensity of the weak streaks was quantitatively analyzed. Figure 4 shows the intensity of the weak streaks, normalized using the (1,0) and (−1,0) streaks, as a function of temperature for various film thicknesses for h-$ScFeO_3$ films grown on both Al_2O_3 and STO substrates. As shown in Fig. 4(a), there is no obvious transition for the intensity of the weak streak for the 2 uc film, so the ferroelectric T_c may be lower than room temperature. All the other films, with thickness ranging from 4 to 41 uc, exhibit a transition of the weak streak intensity above room temperature. More importantly, T_c increases when the thickness increases.

To interpret the key factors determining the thickness-dependent scaling of T_c in ultrathin h-$RFeO_3$ films and the potential critical thickness, we treat the h-$RFeO_3$ near the interface as the interfacial clamping layer, where the magnitude of structural distortion (Q) is

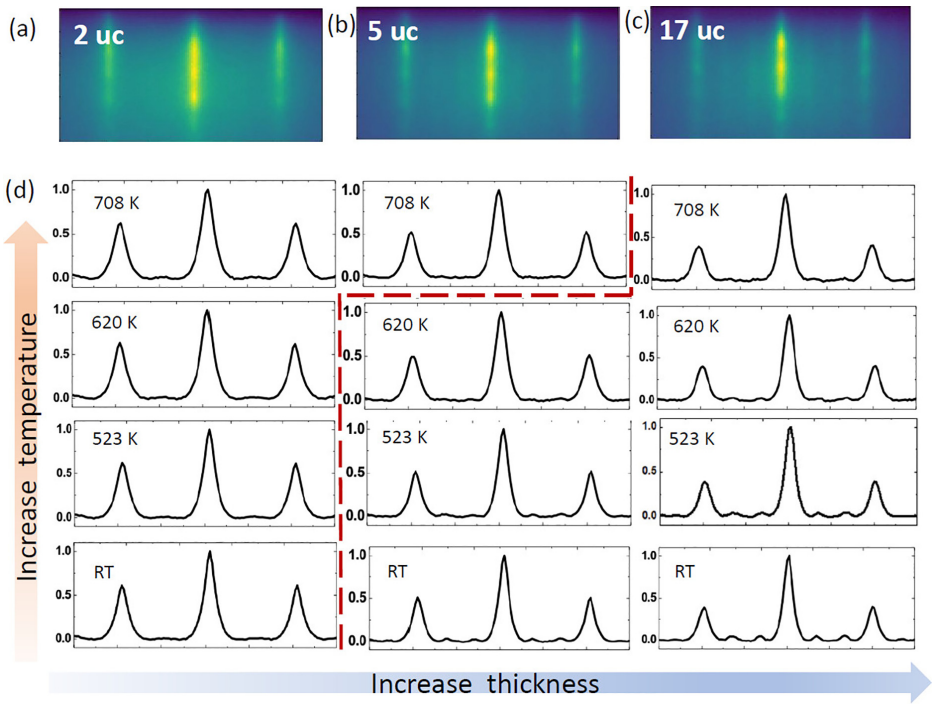

FIG. 3. (a)–(c) RHEED images of h-$ScFeO_3/Al_2O_3$ films with thicknesses of 2, 5, and 17 uc at room temperature. (d) Normalized profiles of the RHEED intensity with different thicknesses and temperatures for h-$ScFeO_3/Al_2O_3$ films. The dashed line indicates the boundary between the paraelectric and ferroelectrics phases.

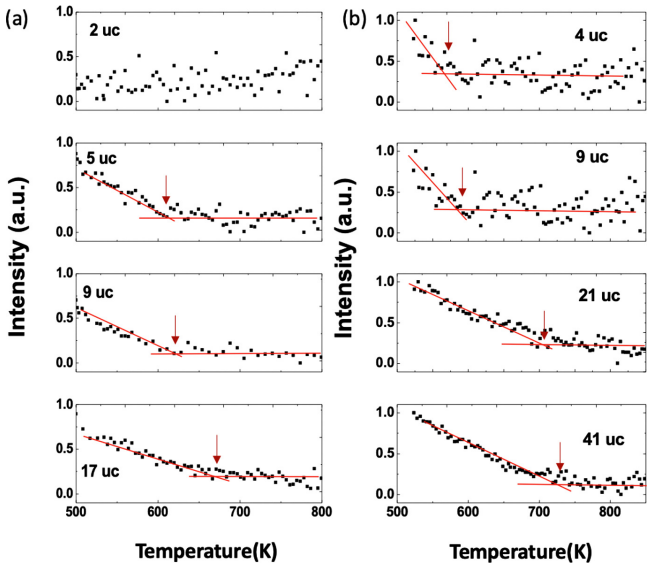

FIG. 4. The temperature-dependent normalized RHEED intensity of (1/3, 0) streak for (a) h-$ScFeO_3$/Al_2O_3 and (b) h-$ScFeO_3$/STO films with different thicknesses.

suppressed completely at the beginning and increases gradually when the rare earth layer is away from the interface. In other words, the boundary condition is fixed at the interface ($Q=0$ at $z=0$) and free at the top surface based on experimental observations.[10,11] Considering the free energy of the structural distortion and the elastic energy at the same time within the framework of the Landau theory[18,24] (see Sec. 2 in the supplementary material), the structural distortion as a function of the thickness and temperature can be written as

$$Q(z,T)=Q(\infty,T)\frac{1-\exp\left(-\frac{z}{\zeta(T)}\right)}{1+\exp\left(-\frac{z}{\zeta(T)}\right)},$$

with

$$\begin{cases} Q(\infty,T)=\sqrt{\frac{-a_0}{b}}\sqrt{1-\frac{T}{T_s}}, \\ \zeta(T)=\sqrt{\frac{k}{-a_0}}\sqrt{\frac{T_s}{T_s-T}}=\zeta_0\sqrt{\frac{T_s}{T_s-T}}, \end{cases} \tag{1}$$

in which z is the distance from the film/substrate interface, T is the temperature, $\zeta_0=\sqrt{\frac{k}{-a_0}}$, $a_0<0$ and $b>0$ are coefficients of the Landau theory, k corresponds to the stiffness coefficient, T_s is the Curie temperature of bulk state, and ζ_0 is the characteristic length of the interfacial clamping layer at $T=0$ K. In Eq. (1), $Q(\infty,T)$ represents the temperature-dependent saturated magnitude of K_3 distortion, which equals $\sqrt{\frac{-a_0}{b}}$ when $T=0$ K. By integrating the energy density with respect to z over the thickness of film (t_F), the total energy can be expressed as

$$F(t_F,T)=-\frac{a_0}{2T_S}C1(t_F,T)\left\{\left[T-\left(T_S+\frac{2kT_S}{a_0}\frac{C2(t_F,T)}{C1(t_F,T)}\right)\right]\times Q(\infty,T)^2+\frac{T_S}{2{*}Q_0^2}\frac{C3(t_F,T)}{C1(t_F,T)}Q(\infty,T)^4\right\}, \tag{2}$$

with

$$\begin{cases} C1(t_F,T)=\int_0^{t_F}\left(\frac{1-\exp\left(-\frac{z}{\zeta(T)}\right)}{1+\exp\left(-\frac{z}{\zeta(T)}\right)}\right)^2 dz, \\ C2(t_F,T)=\int_0^{t_F}\frac{\left(\frac{2}{\zeta}*\exp\left(-\frac{z}{\zeta(T)}\right)\right)^2}{\left(1+\exp\left(-\frac{z}{\zeta(T)}\right)\right)^4} dz, \\ C3(t_F,T)=\int_0^{t_F}\left(\frac{1-\exp\left(-\frac{z}{\zeta(T)}\right)}{1+\exp\left(-\frac{z}{\zeta(T)}\right)}\right)^4 dz. \end{cases} \tag{3}$$

When the coefficient before the $Q(\infty,T)^2$ term is less than zero, minimizing $F(t_F,T)$ results in finite $Q(\infty,T)$ corresponding to the ferroelectric order. At $T=T_C$, this coefficient $\alpha(t_F,T_C)$ is zero, i.e.,

$$\alpha(t_F,T_C)=T_C-T_S\left[1-2\xi_0^2\frac{C2(t_F,T_C)}{C1(t_F,T_C)}\right]=0. \tag{4}$$

The phase diagram of $\alpha(t_F,T)$ is plotted in Fig. 5(a) with $\zeta_0=0.7$ uc and $T_S=688$ K. Since $\alpha(t_F,T)<0$ (>0) corresponds to the ferroelectric (paraelectric) state of the h-$RFeO_3$ films, the curve of $\alpha(t_F,T_C)=0$ indicates that the critical thickness of ferroelectricity increases with temperature, which is consistent with the observation of temperature-dependent corrugation of rare earth layers in the h-$YMnO_3$/YSZ film.[10] Moreover, as implied in Eq. (4), the dependence of T_C on t_F is influenced by both T_S and ζ_0, which are two independent parameters that can be extracted from experimental observations such as *in situ* RHEED patterns in this work. As shown in Fig. 5(b), the experimental T_c of both h-$ScFeO_3$ and h-$YMnO_3$ films decreases with smaller thickness, and the trend is slower in the h-$ScFeO_3$ films. By fitting the experimental data with Eq. (4), we find that $T_s=814\pm183$ K and $\zeta_0=0.93\pm0.44$ uc for the h-$YMnO_3$/YSZ film and $T_s=681\pm28$ K and $\zeta_0=0.68\pm0.18$ uc for the h-$ScFeO_3$ films. The comparison between simulation with experimental results indicates that this model may underestimate the bulk Ts, which is a reminder that this work focuses on elucidating the effect of interfacial clamping on the loss of ferroelectricity below a certain thickness. In other words, the model is meant to apply in both hexagonal ferrites and manganites, but in the thin-film limit.

Based on Eq. (4), the zero-temperature ferroelectric critical thickness (ζ_{FE}) can be defined as the interception of the $\alpha(t_F,T)=0$ curve with the $T=0$ K axis, as shown in Fig. 5(c). The ratio of $\zeta_{FE}/\zeta_0=2.25$ is a fixed value, which is independent of materials (see details in supplementary Sec. 4). This ratio indicates that the absence of ferroelectric critical thickness ($\zeta_{FE}=0$) or unsuppressed corrugation of the initial rare-earth layer in h-$RFeO_3$ or h-$RMnO_3$ films can only exist when

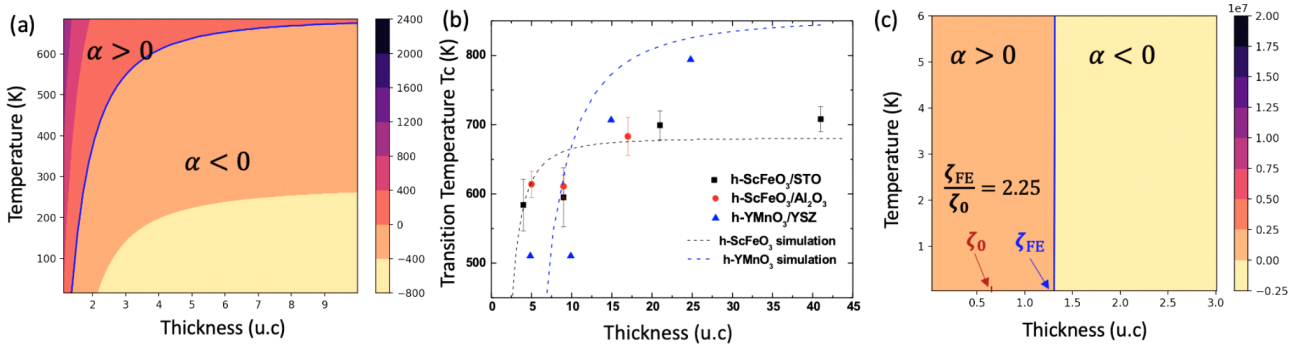

FIG. 5. (a) Calculated phase diagram of coefficient $\alpha(t_F, T)$ in Eq. (4) with temperature and film thickness as independent variables, the blue solid blue line corresponds to $\alpha = 0$. (b) Measured thickness-dependent *Tc* of h-$ScFeO_3$/STO, h-$ScFeO_3$/Al_2O_3, and h-$YMnO_3$/YSZ films and related fitting based on Eq. (4), the data of h-$ScFeO_3$ comes from *in situ* RHEED in this work and the data of h-$YMnO_3$ come from Ref. 10. (c) Phase diagram of α near $T = 0$ K and the comparison of ζ_0 and ζ_{FE}.

there is no interfacial clamping layer ($\zeta_0 = 0$) or when the films become freestanding. Moreover, the improper ferroelectricity under the ultrathin limit could be tuned by choosing the characteristic length of the interfacial clamping layer among different interfaces.

In summary, through quantitative study of *in situ* RHEED patterns during paraelectric-to-ferroelectric phase transition, the thickness-dependent scaling of ferroelectric *Tc* in epitaxial h-$ScFeO_3$ films was revealed. Based on the interfacial clamping mechanism, a phenomenological model from Landau theory was introduced to interpret this scaling behavior and reveal the correlation between the ferroelectric critical thickness and characteristic length of the interfacial clamping layer in ultrathin h-$RFeO_3$ or h-$RMnO_3$ films. These results serve as the guidance to achieve robust improper ferroelectricity in h-$RFeO_3$ through interfacial engineering for future study.

See the supplementary material for more details on x-ray diffraction measurements and modeling using the phenomenological theory.

This work was primarily supported by the National Science Foundation (NSF), Division of Materials Research (DMR) under Grant No. DMR-1454618 and by the Nebraska Center for Energy Sciences Research. The research was performed in part at the Nebraska Nanoscale Facility: National Nanotechnology Coordinated Infrastructure and the Nebraska Center for Materials and Nanoscience, which are supported by the NSF under Grant No. ECCS-2025298 and the Nebraska Research Initiative.

AUTHOR DECLARATIONS

Conflict of Interest

The authors have no conflicts to disclose.

Author Contributions

Xin Li: Conceptualization (equal); Data curation (equal); Formal analysis (equal); Investigation (equal); Visualization (equal); Writing – original draft (equal); Writing – review & editing (equal). **Yu Yun:** Conceptualization (equal); Data curation (equal); Writing – review & editing (equal). **Xiaoshan Xu:** Conceptualization (equal); Data curation (equal); Formal analysis (equal); Funding acquisition (equal); Investigation (equal); Methodology (equal); Project administration (equal); Resources (equal); Software (equal); Supervision (equal); Validation (equal); Visualization (equal); Writing – original draft (equal); Writing – review & editing (equal).

DATA AVAILABILITY

The data that support the findings of this study are available from the corresponding author upon reasonable request.

REFERENCES

[1]M. Osada1 and T. Sasaki, APL Mater. **7**, 120902 (2019).
[2]C. Cui, F. Xue, W.-J. Hu, and L.-J. Li, NPJ 2D Mater. Appl. **2**, 18 (2018).
[3]F. Liu, L. You, K. Seyler *et al.*, Nat. Commun. **7**, 12357 (2016).
[4]D. D. Fong, G. B. Stephenson, S. K. Streiffer *et al.*, Science **304**, 1650–1653 (2004).
[5]D. D. Fong, A. M. Kolpak, J. A. Eastman *et al.*, Phys. Rev. Lett. **96**, 127601 (2006).
[6]C. L. Jia, V. Nagarajan, J. Q. He *et al.*, Nat. Mater. **6**, 64–69 (2007).
[7]J. Junquera and P. Ghosez, Nature **422**, 506–509 (2003).
[8]Y. Hao, T. Li, Y. Yun *et al.*, Phys. Rev. Appl. **16**, 034004 (2021).
[9]N. Sai, C. J. Fennie, and A. A. Demkov, Phys. Rev. Lett. **102**, 107601 (2009).
[10]J. Nordlander, M. Campanini, M. D. Rossell *et al.*, Nat. Commun. **10**, 5591 (2019).
[11]Y. Yun, P. Buragohain, A. S. Thind *et al.*, Phys. Rev. Appl. **18**, 034071 (2022).
[12]Z. Guan, H. He, X. Shen *et al.*, Adv. Electron. Mater. **6**, 1900818 (2020).
[13]K. Chang, T. P. Kaloni, H. Lin *et al.*, Adv. Mater. **31**, 1804428 (2019).
[14]J. Xiao, H. Zhu, Y. Wang *et al.*, Phys. Rev. Lett. **120**, 227601 (2018).
[15]C. Wang, L. You, D. Cobden *et al.*, Nat. Mater. (published online 2023).
[16]X. Li, Y. Yun, A. S. Thind *et al.*, Sci. Rep. **13**, 1755 (2023).
[17]Y. Yun, X. Li, A. S. Thind *et al.*, arXiv:2011.07154.
[18]S. Artyukhin, K. Delaney, N. Spaldin *et al.*, Nat. Mater. **13**, 42–49 (2014).
[19]M. Lilienblum, T. Lottermoser, S. Manz *et al.*, Nat. Phys. **11**, 1070–1073 (2015).
[20]K. Sinha, H. Wang, X. Wang *et al.*, Phys. Rev. Lett. **121**, 237203 (2018).
[21]X. Xu and W. Wang, Mod. Phys. Lett. B **28**, 1430008 (2014).
[22]A. Ichimiya and P. I. Cohen, *Reflection High Energy Diffraction* (Cambridge University Press, 2010).
[23]W. Wang, J. Zhao, W. B. Wang *et al.*, Phys. Rev. Lett. **110**, 237601 (2013).
[24]C. X. Zhang, K. L. Yang, and P. Jia, J. Appl. Phys. **123**, 094102 (2018).